ICSV13 - Vienna
The Thirteenth International Congress on Sound and Vibration
Vienna, Austria, July 2-6, 2006

ACOUSTIC WAVES EMANATING FROM TRANSITIONAL STRUCTURES IN A COMPRESSIBLE BOUNDARY- LAYER FOR HIGH-SPEED TRAIN

Daisuke Watanabe*[1], Hajime Takami[2], Hiroshi Maekawa[1], Katsuhiro Kikuchi[2], Masanobu Iida[2] and Hiroki Suzuki[1]

[1]Graduate School of Engineering, Hiroshima University
1-4-1 Kagamiyama, Higashihiroshima-shi, Hiroshima 739-8527, Japan
[2]Environmental Engineering Division, Railway Technical Research Institute
, Kokubunji-shi, Tokyo, Japan
watanabe@mec.hiroshima-u.ac.jp(e-mail address of lead author)

Abstract

Spatial direct numerical simulations are used to study the formation and development of three-dimensional structures and the resultant sound emission mechanism in a compressible boundary layer, for a high-speed train model, where the free stream velocity of 500Km/h, corresponding Mach number is 0.41. The Reynolds number at the inlet based on the displacement thickness is 1640, which meets the boundary layer of model measurements undergoing transition. In the present work, to overcome the difficulties of the spectral method or pade-type compact schemes for compressible free-shear flows at high Reynolds numbers, the spectral-like finite difference high-order upwind-biased compact schemes (Deng, Maekawa & Shen 1995)[1] are employed. A 4th order Runge-Kutta scheme is used for time advancement. Boundary conditions based on characteristic analysis for the Navier-Stokes equations (Poinsot & Lele 1992)[2] are used so that acoustic waves are not reflected back into the domain. Random disturbances/T-S waves of compressible isotropic turbulence are superimposed on the laminar profile at the inlet plane of the boundary layer computational box. The magnitude of random disturbance is 3% of the free stream velocity. Rapid growth of oblique modes due to second instability of the laminar boundary layer with the amplified T-S waves produces peak-valley splitting structures downstream and later hairpin vortices (hairpin packet) on a low speed streak are observed. Simulation results show that the further complex development of the hairpin vortices lead to vortex interactions of the deformed hairpin vortices, which is responsible to sound generation in the transitional compressible boundary layer. The development of the peak-valley splitting structures is similar to the incompressible boundary layer measurements by Kachanov et al. (1984)[3]. Further comparisons of sound pressure levels between the numerical results and experimental data obtained by a moving model facility for high-speed 500km/h train will be made.

INTRODUCTION

Recently, with the new noise regulations, reducing acoustic noise emissions has become major challenge for high-speed train designers and manufactures. When a high-speed train runs in an open section, where the train speed is in a compressible flow regime, intense acoustic noise is found to radiate from the train. The turbulent boundary layers developing on the train body are considered as one of the major acoustic noise source, especially low-frequency noise source. However, for instances, the study of compressible turbulent boundary layers has primarily consisted of experimental investigations with a few recent attempts at numerical simulation. The experimental measurements are limited to basic turbulent quantities and by spatial resolution near the wall, among other difficulties. The simulations have hampered by large cost and low Reynolds number. Recently, a few direct numerical simulations of compressible turbulent boundary layers have been performed by Rai et al.[1], Piozzolii et al.[2] and others. They have not presented acoustic fields in their simulations. Due to the acoustic field nature, a spatially developing direct numerical simulation rather than temporal formulations is favourable to analyse the acoustic field and boundary layer development of the simulation.

In this paper, we present a direct numerical simulation of spatially developing boundary layer undergoing laminar-turbulent transition and its sound field and show some fundamental results obtained from simulation database. Although this approach is too computationally intensive to be employed as a predictive tool, it is uniquely capable of providing information of both the flowfields and sound fields. The fully compressible Navier-Stokes equations were solved in cylindrical coordinates to present the boundary layers developing on the train body. .

NUMERICAL METHODS

In the direct numerical simulations, the nondimensional equations governing the conservation of mass, momentum, and energy for a compressible Newtonian fluid are solved using fifth-order dissipative compact finite difference schemes Deng1996[1] in all directions. The governing equations in cylindrical coordinates are given as follows;

$$\frac{\partial \rho}{\partial t} + \frac{1}{r}\frac{\partial (r\rho u_r)}{\partial r} + \frac{1}{r}\frac{\partial (\rho u_\theta)}{\partial \theta} + \frac{\partial (\rho u_x)}{\partial x} = 0\,, \tag{1}$$

$$\frac{\partial (\rho u_r)}{\partial t} + \frac{1}{r}\frac{\partial (r\rho u_r u_r)}{\partial r} + \frac{1}{r}\frac{\partial (\rho u_r u_\theta)}{\partial \theta} + \frac{\partial (\rho u_r u_x)}{\partial x} - \frac{\rho u_\theta u_\theta}{r} = -\frac{\partial p}{\partial r} + \left[\frac{1}{r}\frac{\partial (r\tau_{rr})}{\partial r} + \frac{1}{r}\frac{\partial \tau_{r\theta}}{\partial \theta} - \frac{\tau_{\theta\theta}}{r} + \frac{\partial \tau_{rx}}{\partial x}\right], \tag{2}$$

$$\frac{\partial(\rho u_\theta)}{\partial t}+\frac{1}{r}\frac{\partial(r\rho u_r u_\theta)}{\partial r}+\frac{1}{r}\frac{\partial(\rho u_\theta u_\theta)}{\partial \theta}+\frac{\partial(\rho u_\theta u_x)}{\partial x}+\frac{\rho u_r u_\theta}{r}$$
$$=-\frac{1}{r}\frac{\partial p}{\partial \theta}+\left[\frac{1}{r^2}\frac{\partial(r^2\tau_{\theta r})}{\partial r}+\frac{1}{r}\frac{\partial \tau_{\theta\theta}}{\partial \theta}+\frac{\partial \tau_{\theta x}}{\partial x}\right], \quad (3)$$

$$\frac{\partial(\rho u_x)}{\partial t}+\frac{1}{r}\frac{\partial(r\rho u_r u_x)}{\partial r}+\frac{1}{r}\frac{\partial(\rho u_\theta u_x)}{\partial \theta}+\frac{\partial(\rho u_x u_x)}{\partial x}$$
$$=-\frac{\partial p}{\partial x}+\left[\frac{1}{r}\frac{\partial(r\tau_{xr})}{\partial r}+\frac{1}{r}\frac{\partial \tau_{x\theta}}{\partial \theta}+\frac{\partial \tau_{xx}}{\partial x}\right], \quad (4)$$

$$\frac{\partial Et}{\partial t}+\frac{1}{r}\frac{\partial[r(Et+p)u_r]}{\partial r}+\frac{1}{r}\frac{\partial[(Et+p)u_\theta]}{\partial \theta}+\frac{\partial[(Et+p)u_x]}{\partial x}$$
$$=\frac{1}{r}\frac{\partial(ru_i\tau_{ir})}{\partial r}+\frac{1}{r}\frac{\partial(u_i\tau_{i\theta})}{\partial \theta}+\frac{\partial(u_i\tau_{ix})}{\partial x}+\frac{1}{r}\frac{\partial}{\partial r}\left(\kappa r\frac{\partial T}{\partial r}\right)+\frac{1}{r^2}\frac{\partial}{\partial \theta}\left(\kappa\frac{\partial T}{\partial \theta}\right)+\frac{\partial}{\partial x}\left(\kappa\frac{\partial T}{\partial x}\right), \quad (5)$$

where

$$E_t=\frac{p}{(\gamma-1)}+\frac{\rho\, u_x u_x}{2}+\frac{\rho\, u_r u_r}{2}\frac{\rho\, u_\theta u_\theta}{2}, \quad \mathbf{(6)}$$

$$\tau_{xx}=\frac{\mu}{\mathrm{Re}}\left\{\left(2\frac{\partial u_x}{\partial z}\right)-\frac{2}{3}\left[\frac{1}{r}\frac{\partial(ru_r)}{\partial r}+\frac{1}{r}\frac{\partial u_\theta}{\partial \theta}+\frac{\partial u_x}{\partial x}\right]\right\},\ \tau_{xr}=\tau_{rx}=\frac{\mu}{\mathrm{Re}}\left(\frac{\partial u_r}{\partial x}+\frac{\partial u_x}{\partial r}\right),$$

$$\tau_{rr}=\frac{\mu}{\mathrm{Re}}\left\{\left(2\frac{\partial u_r}{\partial r}\right)-\frac{2}{3}\left[\frac{1}{r}\frac{\partial(ru_r)}{\partial r}+\frac{1}{r}\frac{\partial u_\theta}{\partial \theta}+\frac{\partial u_x}{\partial x}\right]\right\},\tau_{r\theta}=\tau_{\theta r}=\frac{\mu}{\mathrm{Re}}\left[r\frac{\partial}{\partial r}\left(\frac{u_\theta}{r}\right)+\frac{1}{r}\frac{\partial u_r}{\partial \theta}\right],$$

$$\tau_{\theta\theta}=\frac{\mu}{\mathrm{Re}}\left\{\left[2\left(\frac{1}{r}\frac{\partial u_\theta}{\partial \theta}+\frac{u_r}{r}\right)\right]-\frac{2}{3}\left[\frac{1}{r}\frac{\partial(ru_r)}{\partial r}+\frac{1}{r}\frac{\partial u_\theta}{\partial \theta}+\frac{\partial u_x}{\partial x}\right]\right\},\tau_{\theta x}=\tau_{x\theta}=\frac{\mu}{\mathrm{Re}}\left(\frac{1}{r}\frac{\partial u_x}{\partial \theta}+\frac{\partial u_\theta}{\partial x}\right), \quad (7)$$

$$\kappa=-\frac{\mu}{(\gamma-1)M^2 RePr}, \quad (8)$$

$$T=\frac{\gamma M^2 p}{\rho}, \quad (9)$$

$$\mu=T^{2/3}, \quad (10)$$

$M=U/c_\infty$ and c_∞ is the speed of sound at the freestream. The all variables, in all the following discussions, are nondimensionalized by the characteristic physical scales such as freestream velocity U, density ρ_∞, temperature T_∞ and inlet displacement thickness of δ_0^*.

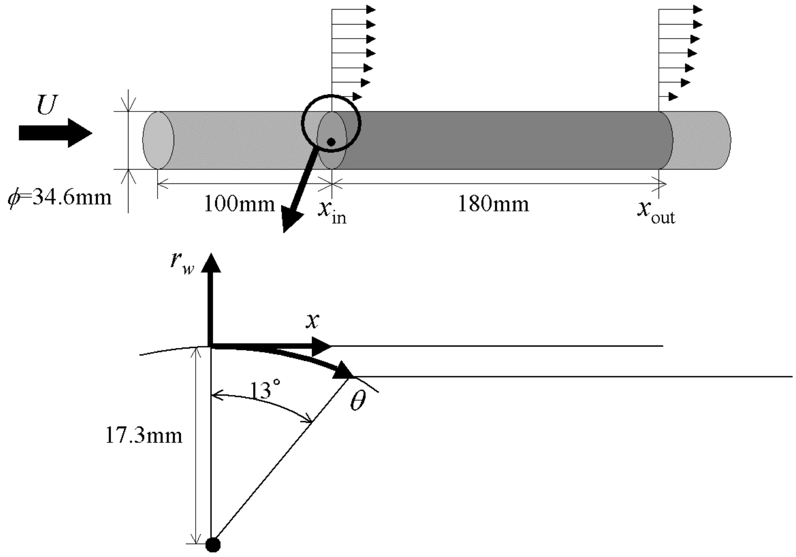

Figure 1– Computational box

$$Re = \frac{U\delta_0^*}{\mu_\infty}. \tag{11}$$

We employed the mean streamwise velocity profile given by the Blasius boundary layer at the inlet. The mean temperature was calculated with the Crocco-Busemann relation for unity Prandtl number;

$$\overline{T}(y) = M^2 \frac{\gamma - 1}{2}(U\overline{u}(y) - \overline{u}(y)^2) + \frac{T_w(U - \overline{u}(y))}{U} + \frac{T_\infty \overline{u}(y)}{U}, \tag{12}$$

where γ is the ratio of specific heats. The wall is isothermal wall and wall temperature is $T_w = 1$.

For 3-D spatial DNS, the computational mesh was $N_x \times N_r \times N_\theta = 601 \times 151 \times 48$. Mesh points were compressed in the streamwise and radial directions.

NSCBC (Navier-Stokes Characteristic Boundary Conditions)[2] were implemented in the treatment of the boundaries at the in/outflow and far radial regions. Periodic boundary conditions were implemented in the azimuthal directions. Outflow boundaries were located in $x = 180\,\text{mm}(= 1000\delta_0^*)$ for streamwise, $r_w = 10\,\text{mm}(= 57\delta_0^*)$ for radial and $\theta = 13^\circ$ for the azimuthal direction (see figure 1). The boundary layer developing on the cylinder of r=17.3mm is calculated.

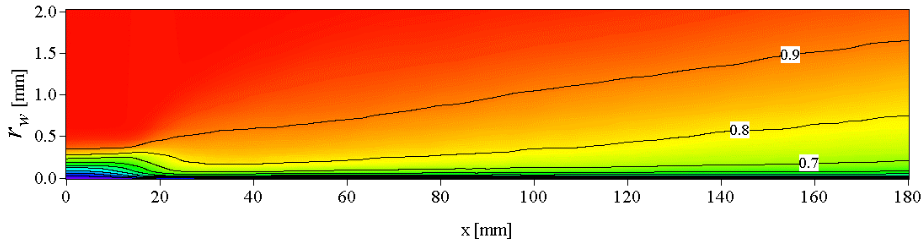

Figure 2 – Mean streamwise velocity $\overline{u}\,/\,U$

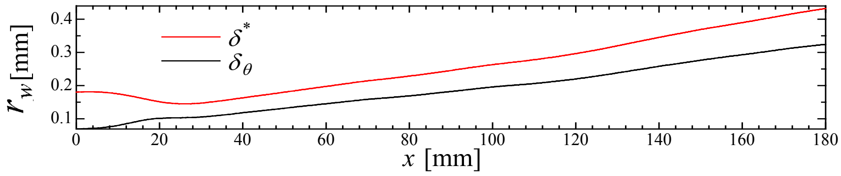

Figure 3 – Downstream development of displacement thickness and momentum thickness

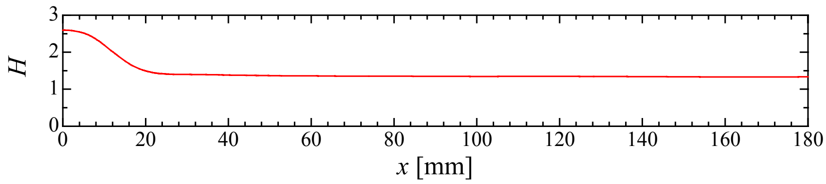

Figure 4 – Downstream development of shape factor

RESULTS

Mean flow

Spatial DNS with random velocity forcing at the inlet for M=0.41 (U=500km/h), $Re_{\delta_0^*} = 1640$ and $\delta_0^* = 0.18\,\text{mm}$ is performed to investigate the flow structure and noise generation. The root mean square of velocity disturbance was 3% of the free stream velocity U.

Figures 2, 3 and 4 show the characteristic of mean streamwise velocity. The contour plots of the mean streamwise velocity shown in figure 2 clearly indicate a change of the flow pattern. At the locations of x<10mm, due to the inflow disturbance that does not fit the flow, the mean flow pattern is almost a laminar state. Along the down stream location, the flow pattern varies greatly because chosen disturbances affect the boundary layer. For x>30mm, the mean velocity profile spreads outside gradually. A change of the displacement thickness δ^* and the momentum thickness δ_θ shown in figure 2 is rapid for x<30mm. After x=30mm, δ^* and δ_θ shows a greatly increase. The shape factor H is 1.4 for x>30mm and almost keeps a constant value. Therefore, these results suggest that the flow becomes turbulent boundary layer for x>30mm.

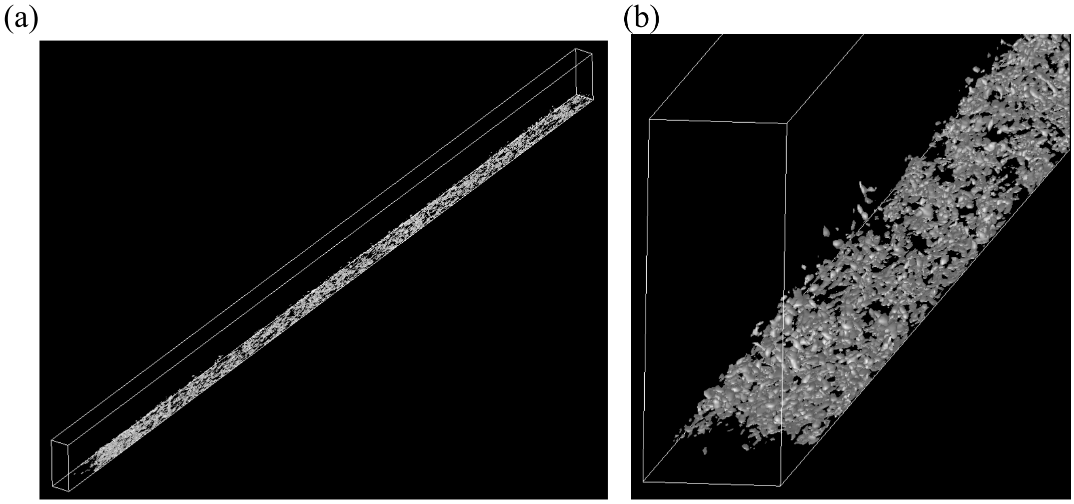

Figure 5 – Vortex structure; (a) all computational domain and (b) expansion view at the inlet

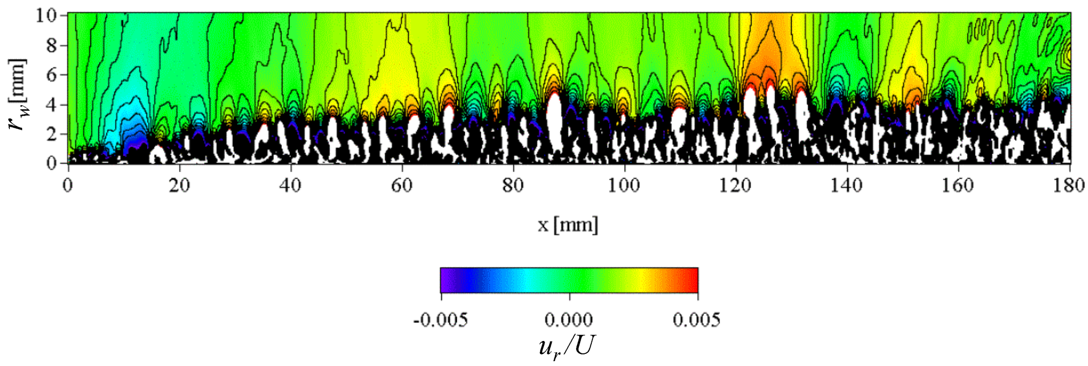

Figure 6 – Radial velocity u_r/U

Flow structures

Figure 5 shows the downstream development of the vortical structures. The structure is visualized with iso-surfaces of the second invariant Q of the velocity gradient tensor. These figure show that vortical structures develop at the locations of x>10 where the shape factor begins decrease (see figure 4) and the developed vortical structures are distributed on a wall surface down stream. Additionally, we can see the fine vortical structures in the boundary layer.

Figure 6 presents a snapshot of the radial velocity fields at the $\theta = 0^\circ$ plane. The waves with long-wavelength observed outside of the boundary layer, as shown in the coloured region of Fig.6, then the waves with short wavelength locate at near wall region, as shown in the black and white coloured region of Fig.6. These wavelengths are clearly different. The short waves located near the wall are found to be association with fine vortilcal structures, as shown in figure 5. On the other hand, the longer waves may be caused by large-scale vortical structure in turbulent boundary layer.

In figure 9, radial directional distribution of power spectra related to radial velocity at x=25.5mm and x=133.4mm are visualized. These figures show that there are

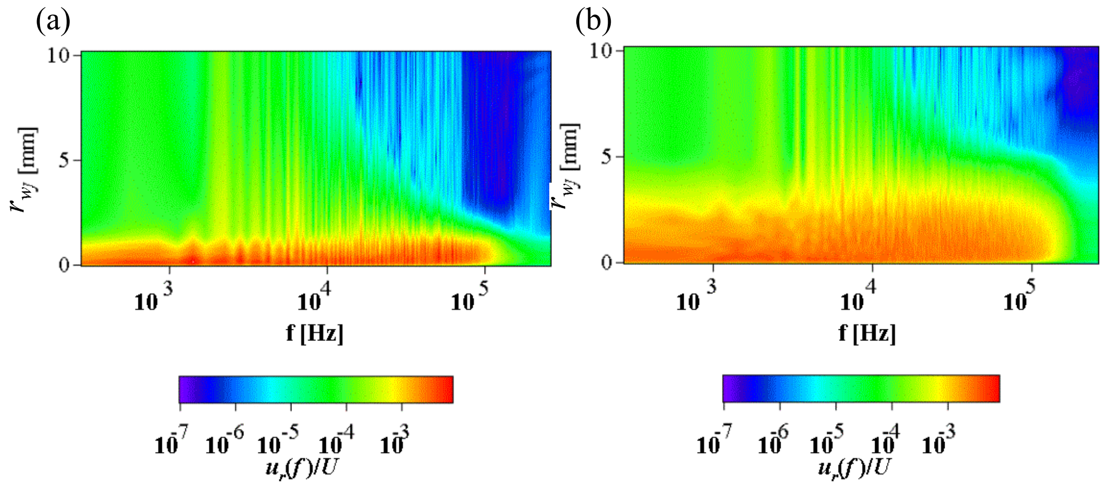

*Figure 7– Radial directional distribution of radial velocity spectrum $u_r(f)/U$ at (a) $x=25.5$*mm *and (b) $x=133.4$*mm

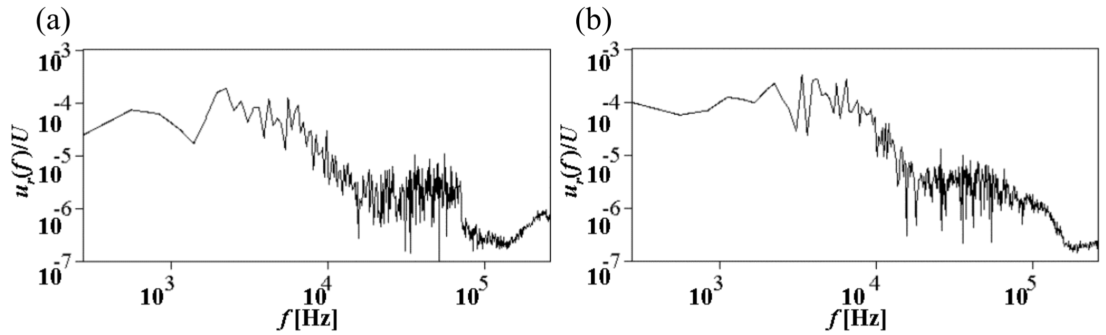

Figure 8 – Radial velocity spectrum at $r_w=10$ mm; *(a) $x=25.5$* mm *and (b) $x=133.4$* mm

two different types of waves. First type is the waves that have a wide spectrum in the near wall region. Second type is waves that have "discrete" spectral. The waves with wide spectrum have the characteristic that, amplitude distribution is almost limited in inner boundary layer. As shown in Figure 7(a), the region that magnitudes are of 10^{-3} order, distributes inside r_w<1mm for x=25.5mm and distribute inside r_w<4mm for x=133.4mm. These ranges are in proportion to displacement thickness (see figure 3). On the other hand, the amplitude of the wave with "discrete" spectrum distribution spreads outside of the boundary layer. Existence of this wave ensures the fact that long waves observed in figure 6 are generated with a constant period and travel along the boundary layer down stream. Note that the fluctuation observed here expresses velocity fields with vortical structures instead of sound waves.

Figure 8 shows the radial velocity spectral that same streamwise location in Figure 7 at r_w=10mm. These figures show that there are the "discrete" low frequency waves at x=25.5mm, and the waves are generated in the transitional region (10<x<30). Furthermore, although these spectral distribution is somewhat different from at x=25.5mm in at x=133.4mm, the "discrete" low frequency is almost observed between 10^3 and 10^4.

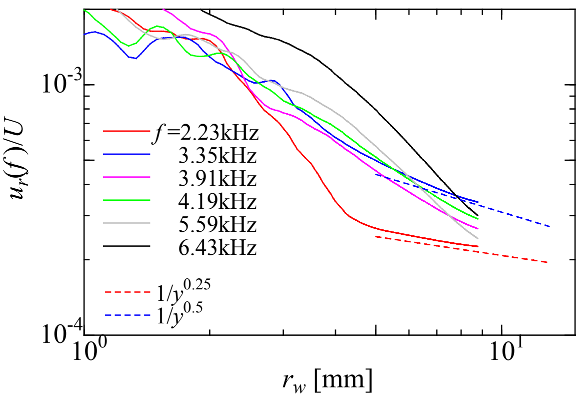

*Figure 9 – Profiles of radial velocity spectrum $u_r(f)/U$ at x=133.4*mm

The amplitude profiles of the "discrete" low frequency at x=133.4mm are shown in figure 9. This figure shows that these amplitude decreases with increase of r_w. Note that this change of the amplitude is not a monotonous decrement (see f=2.23kHz at r_w=40 in figure 9). This matter shows that the distributions of amplitude for f=2.23kHz and f=3.35kHz are stack of the wave with discrete low frequency and the wave with wide spectra. Furthermore, with the decrease of frequency, the dumping factor of amplitude is decrease, as for f=2.23kHz is $1/y^{0.25}$ and for f=3.35kHz is $1/y^{0.5}$. Therefore, it is supposed that the low frequency amplitude is still large far radial region. In addition, far fields of the boundary layer, the spectrum may be dominated by the low frequency.

SUMMARY (OR CONCLUSIONS)

Spatial DNS of a cylindrical boundary layer for the free stream of U=500km/h has been performed. The numerical results provide new physical insights into flow field in a cylindrical turbulent boundary layer. There are two different types of waves. First one is the wave that has a wide spectrum in the near wall region. Second one is the wave that has a discrete spectral. The wave of "discrete" spectral decreases gradually with the increase of frequency. Therefore, far fields of the boundary layer, the spectrum may be dominated by the low frequency.

REFERENCES

[1| Deng, X., Maekawa, H. & Shen, C., "A class of high-order dissipative compact schemes", AIAA Paper 96-1972, (1996).

[2] Poinsot, T. J. & Lele, S. K., "Boundary conditions for direct simulation of compressible viscous flows", J. Comput. Phys. **101**, 104-129 (1992).

[3] Kachanov, Y. S. & Levchenko, V. YA., "The resonance interaction of disturbances at laminar-turbulent transition in a boundary layer", J. Fluid Mech. 138, 209-247 (1984).